THE JOURNAL OF PHYSICAL CHEMISTRY A

 VOLUME 108, NUMBER 36, SEPTEMBER 9, 2004

ARTICLES

Anomalously Slow Diffusion of Single Molecules near a Patterned Surface

Erwen Mei,[†] Alexey Sharonov,[†] Feng Gao,[†] James H. Ferris,[‡] and Robin M. Hochstrasser*[,†]

Departments of Chemistry and of Materials Science and Engineering, University of Pennsylvania, Philadelphia, Pennsylvania 19104

Received: April 23, 2004; In Final Form: June 28, 2004

Two-dimensional hexagonal arrays of micrometer-sized spheroidal cavities were fabricated from poly(vinyl alcohol) films on microscope cover glasses. The patterned surfaces in contact with solution and another regular cover glass were used to contain single molecules. Bursts of fluorescence from a series of single molecules entering and leaving the beam focus were observed. The molecules were all rotating rapidly compared with the fastest binning time of 100 μs. The fluorescence anisotropy decayed on the nanosecond time scale. The fluorescence spectra of mixtures of dyes confirmed that the bursts separated by time intervals of several to tens of seconds are from different molecules, while those bursts spanning intervals of several to tens of milliseconds are from the same molecule continually reentering the focus. The autocorrelation function of the time-resolved fluorescence intensity suggests a translational diffusion coefficient of 1.7×10^{-8} cm^2 s^{-1} for 6-carboxyrhodamine 6G hydrochloride molecules near the pattern, which is ~260 times smaller than that in free solution. The mechanism of slowing the transverse diffusion process of single molecules near the pattern was further elucidated by total internal reflection microscopy, from which the molecules were observed to be avoiding the cavities.

Introduction

The development and application of techniques for detecting, characterizing, and manipulating single molecules has been one of the important efforts in the area of chemistry and physics within the past decade.[1−6] Single-molecule measurements are no longer technological demonstrations but are employed to acquire properties of materials and biological systems that are not readily obtainable by ensemble measurements.[7−11] The single-molecule method based on laser confocal fluorescence microscopy is a common experimental approach. The single molecules are detected either when they are immobilized at the focus of the microscope or when they are freely diffusing through the confocal region of the focused laser. In both cases molecules reside in the probe volume for a certain period, and it is advantageous to make this time as long as possible.[12]

Several effective single-molecule immobilization techniques have been employed, such as attaching them to surfaces by charge attraction,[10] tethering them to surfaces through chemical bonds,[13] or encapsulating molecules in viscous materials.[9,14,15] However, the behavior and properties of such immobilized single molecules may be modified from those in free solution by the encapsulating material. There are numerous examples of such variations for dye molecules.[14,16] In another example, the conformational dynamics of single immobilized peptides were shown to be influenced by proximity to a surface, even in buffered solutions on chemically modified surfaces.[17] Single molecules that are free in solution have also been detected while they diffuse through the focus of the laser beam.[5,18] This method, which is based on correlation spectroscopy, has been used to study the diffusion process of single molecules in solution,[19−22]

* To whom correspondence should be addressed.
[†] Department of Chemistry.
[‡] Department of Materials Science and Engineering.

10.1021/jp0482161 CCC: $27.50
Published on Web 08/11/2004

and to investigate the folding and unfolding dynamics of proteins, peptides, and DNA.[17,23,24] In a recent advance, a microfabricated laminar-flow mixer was coupled to a confocal microscope[12] and the FRET efficiencies of individual dye-labeled protein molecules were obtained as they flowed through the probe volume at selected times.

While the free-diffusion single-molecule method does offer a very effective way to study molecules that are not perturbed by surfaces, the observation time window is limited. The residence time τ of a molecule in a spherical cavity of diameter R is $\langle R^2 \rangle / 6D$, where D is the diffusion coefficient.[18] For rhodamine 6G (Rh6G) in water,[25] $D = 2.8 \times 10^{-6}$ cm^2 s^{-1}, so for $R = 500$ nm, which is comparable with the $1/e^2$ diameter of a focused laser beam, τ is $\sim$150 μs. It would be desirable to record signals from each single molecule for much longer than this. However, for the strong emitter Rh6G at 1.0 mW laser power yields only $\sim$1 detected photon/μs in a confocal arrangement. Therefore, only $\sim$150 photons can be obtained per burst in the correlation mode, which does not allow all the properties of interest from a single molecule to be obtained with suitable accuracy. For example, it is not enough for a definitive spectrum even using the most sensitive CCD camera. For a lifetime measurement, assuming a background-free monoexponential decay, about 185 photons are required.[26] To determine whether a decay is or is not exponential, many more photons ($\sim$400000)[26] are needed. Furthermore, there is always a background signal in single-molecule experiments. The count rate can be increased by increasing the excitation power, but at some point the emission rate becomes independent of power because of the finite fluorescence lifetime. For Rh6G, a diffraction-limited beam at 1 mW is already close to the saturation intensity. Furthermore, with a more intense laser the time taken to photobleach a molecule is decreased, which reduces the total observation time.[22] In free-diffusion single-molecule experiments, the excitation power is often varied from several hundred microwatts to more than 1 mW, whereas for immobilized molecules about 1 μW or less is typically required to obtain a good signal-to-noise ratio.[27−30] While the free-diffusion single-molecule method has the significant advantage of being surface free, it is important to find methods which can slow the diffusion of molecules in solution, especially for studying single biomolecules in physiological environments. Attaching the molecules to larger particles that diffuse more slowly may sometimes be useful, but the presence of a possibly perturbing surface is reintroduced by the drag.

In the present work, patterned surfaces were fabricated using methods that had been developed for obtaining ordered three-dimensional arrays of spherical cavities.[31−35] Similar two-dimensional arrays of spherical cavities have been used to restrict Brownian motion of single DNA molecules within cavities.[36] The question we explore in this study is how the patterning of the surface influences the diffusion of molecules in the solution in contact with it.

Materials and Methods

Materials. Samples were prepared from commercially available poly(vinyl alcohol) (PVA; MW $\approx$ 108000, hydrolyzed 99.7%, Polysciences), chloroform, and methanol (both HPLC grade, Fisher Scientific). All materials were used as received. Aqueous suspensions of polystyrene microspheres (Polysciences) were used for patterning. Spheres with average diameters of 0.5 and 1 μm were employed in separate experiments. The polymer and microspheres were spin cast onto microscope cover glasses, which had been rigorously cleaned by sonication in 0.3 M NaOH, deionized water, 2% H_2SO_4, and deionized water then dried under nitrogen. 6-Carboxyrhodamine 6G hydrochloride (Rh6G), tetramethylrhodamine ethyl ester perchlorate (TMR), and TMR−dextran (all from Molecular Probes) were used as single-molecule probes. The concentrations of the sample solutions were all in the range of 0.1 nM.

Time-resolved fluorescence anisotropy experiments were carried out by a conventional time-correlated single-photon-counting method combined with the microscope system described below. A Nd:YAG, operating at 76 MHz, was to generate the 532 nm pulses used in the experiments. The commercial software FluoFit (PicoQUANT) was used to fit the time-resolved anisotropy data.

Microscopy. The scanning confocal microscope, described previously,[37] uses a sample-scanning stage (Queensgate) with closed-loop $X-Y$ feedback for accurate sample positioning and location of individual molecules. The stage is controlled by a modified Nanoscope E controller (Digital Instruments). The sample and stage were mounted on an inverted, epiilllumination microscope (Nikon, Diaphot 300). The 514.5 nm line of an argon ion laser was circularly polarized and used to excite the samples. The excitation power was maintained in the range of 3−50 μW. A Nikon FLUOR 40×, 1.3 numerical aperture (NA) objective was used to produce a nearly diffraction limited focus on the sample and to collect the fluorescence. Appropriate combinations of notch (Kaiser Optical), band-pass, long-pass, and dichroic filters (Chroma Technology) were used to spectrally isolate the signals. Two single-photon-counting avalanche diodes detected the photons reflected and transmitted by a polarizing beam splitter, thereby isolating the fluorescence emitted by the molecules into orthogonal polarization directions, s and p, in the focal plane of the objective. The fluorescence spectra of single molecules were obtained by means of a monochromator (Acton Research) equipped with a back-illumination liquid nitrogen cooled CCD camera (Princeton Instruments, Trenton, NJ).

The microscope for total internal reflection fluorescent microscopy (TIRFM) was based on a commercial Olympus IX81 inverted microscope. The laser beam from an Ar^+ ion laser (National Laser Co., 514.5 nm) passes through a $\lambda/4$ plate to generate circularly polarized light which is then focused by lenses onto the back focal plane of a microscope oil-immersion objective (Olympus, 60×, NA = 1.45). The lens, coupled with a translation stage, was used to align the excitation beam across the objective's back aperture to achieve easy illumination, angle adjustment, and interconversion of the setup between through-the-objective TIRFM and epifluorescence microscopy. The glass coverslides' (Fisher Scientific) refractive index ($n = 1.53$ at 500 nm) matches perfectly PVA's index of refraction ($n = 1.53$), and the critical angle for the PVA−methanol ($n = 1.33$) interface was 60.4°. The excitation spot was 30−85 μm in diameter. The maximum incident intensity at the sample plane was 0.75 kW/cm^2, although in many experiments it was attenuated to much lower values to minimize the photobleaching. The excitation was filtered by a laser band-pass filter and a dichroic mirror (Chroma). The fluorescence from the sample was collected by the objective and directed to a CCD camera with multiplication on chip capability (Roper Scientific, Cascade 512F) by means of a beam splitter and an appropriate set of filters (540LP and 630SP, Omega Optical). With the 1.6× lens the total magnification of the microscope was 96×, which corresponds to a pixel size in the image plane of 167 nm. Specially designed LabView (National Instruments) based software was developed to record sequences of images with

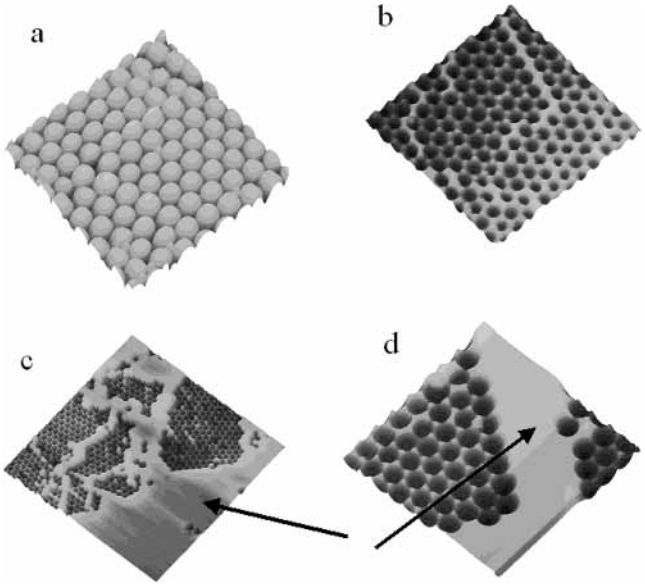

Figure 1. Topographic AFM images of the patterned surface at intermediate steps during its fabrication: (a) image of the monolayer of 1 μm polystyrene spheres on a glass substrate; (b−d) images of the PVA network and templates remaining after solvent extraction of the 1 μm spheres (c, d) and 0.5 μm spheres (b). The arrows in (c) and (d) indicate the polymer wall surrounding the pattern. Image size: (a) 8.4 × 8.4 μm; (b) 6 × 6 μm; (c) 30 × 30 μm; (d) 10 × 10 μm.

various exposure times (typically 20−50 ms in our experiments) and a maximum possible collection rate of 27 frames/s for the whole (512 × 512 pixels) image frame. The signal-to-background ratio in most of the experiments was 12−15, so easy discrimination of single-molecule fluorescence was possible. MatLab (Mathworks Inc.) based software was used for image analysis.

All atomic force microscopy (AFM) images were obtained using the Digital Instruments Dimension 3000 SPM equipped with the Nanoscope IIIa controller. The AFM tips used were commercially available non-contact-etched silicon probes from MicroMasch (NCS15, force constant ∼40 N/m). All images were collected in intermittent contact mode. Images were corrected by plane fitting and are shown unfiltered.

Surface Pattern Fabrication. Approximately 20 μL samples of aqueous suspensions of polystyrene microspheres were deposited on a clean microscope cover glass. The samples were then spin cast to form a thin film. A monolayer or multilayer array of spheres is formed on the cover glass, in agreement with previous reports.[31,34,35] Only monolayer films, as identified by optical microscopy, were selected for the next step. The microsphere-coated substrates then were dried at room temperature for ∼24 h. They were subsequently coated with a thin layer of PVA by spin casting 20 μL of PVA aqueous solution (2.5% by weight) and redried at room temperature for another ∼24 h. Figure 1a shows a typical image of an ordered array of spheres obtained by intermittent contact mode AFM. The addition of water-soluble polymer to the dried monolayer and subsequent spin casting did not substantially disorder these arrays. According to the observations by optical microscopy and the AFM images, ordered regions with sizes ranging from several tens to several hundreds of micrometers are easily fabricated by this method.

The dried arrays of spheres in PVA on cover glasses were then soaked in chloroform for ∼24 h to remove the polystyrene. The films were then dried in air for ∼10 h. Figure 1b shows the AFM image of the template that remains in the PVA films after dissolution of the microspheres. The total height of the polymer features as measured by AFM was 300 nm to 1 μm, depending on the location within the film. As shown in Figure 1b,c, in the locations where there is disorder, the films are thicker than in the surrounding ordered areas. The formation of those ordered regions is consistent with the polymer solution having penetrated into the interstitial voids between the polystyrene spheres. The synthesis and mechanism of formation of similar meso- or macroporous materials have been described in several reports where more information can be obtained.[31−35,38] The focus of the present work is on the role of the polymer network in altering the motion of single molecules.

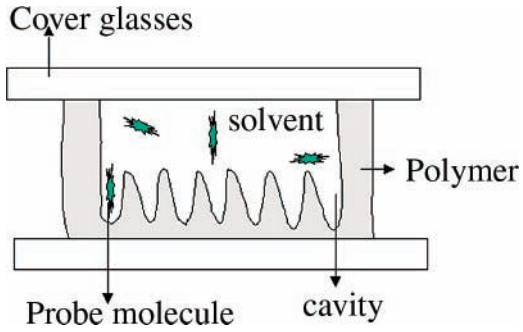

Figure 2. Schematic of the sample prepared by the method described in the text and used in our experiments. The probe molecules and solvent are trapped by two cover glasses and the surrounding polymer wall visualized in Figure 1c,d. Molecules are detected only when they diffuse through the focus of the laser beam.

To photobleach as many impurities as possible and improve the single-molecule detectability, the cover glasses with the patterns were immersed in a methanol sonication bath for ∼30 min and then exposed to a multiline argon laser for ∼3 h at a laser power of ∼3 W/cm^2. The cover glass was mounted on the sample scanning stage with the template facing upward. The outline of the network was visible under the optical microscope so the cover glass could be moved to positions where the laser focus was on an ordered region. These procedures were repeated until the background signal was less than ∼400 counts/s. At that point, 5 μL of sample solution was added to the template, which was then capped with another clean cover glass. Figure 2 shows a cartoon of the sample structure used in the single-molecule experiments. As shown in Figure 1c,d, the patterned polymer regions are completely surrounded by a wall of polymer. This wall, which defines the crater of patterned surface, is important in preventing evaporation of the methanol. So some samples remained viable for hours, whereas it took less than ∼10 min for 5 μL of methanol sandwiched between two cover glasses to dry as evidenced by the immobilization of the single molecules.

Results and Discussion

Single-Molecule Detection and Characteristics. When the laser was focused onto the center of one of the patterned regions and the fluorescence signal collected in two orthogonal polarization directions, the typical fluorescence intensity−time records collected time bins of 1 ms and 100 μs as shown in Figure 3. These records contain a series of photon bursts, each corresponding to a molecule traversing the probe volume defined by the focus of the laser. The bursts are separated by relatively longer periods where there is no emission. The length of the dark period between two bursts corresponds to the time between a molecule exiting and another, or the same one, reentering the probe volume. This period should depend on the concentration of the sample and may also be affected by optical trapping.[39]

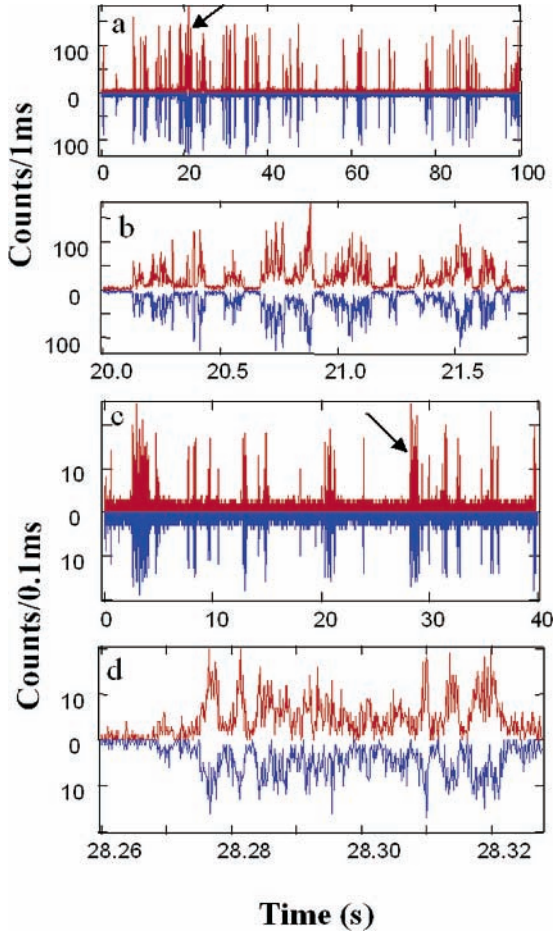

Figure 3. Typical fluorescence intensity−time records of single Rh6G molecules diffusing in methanol through the laser focal region obtained with the same excitation powers of 40 μW, but different integration times: (a) integration time of 1 ms; (b) expanded view of the burst indicated by the arrow in Figure 1a; (c) integration time of 100 μs; (d) expanded view of the burst indicated by the arrow in Figure 1c. The patterned surface used here was created with 0.5 μm spheres.

As shown in Figure 3, the fluorescence fluctuations are nearly identical in the two polarization channels. This result indicates the molecules are rotating during the measurement. The signals in the two channels are not expected to be identical even if there is free rotation because of alignment, nonideal optical elements, and the different quantum efficiencies of the two detectors. These factors might account for some of the small differences in signals from the two channels. The molecular rotation can be assessed from measurements of the dichroism $A(t)$, which is defined as

$$A(t) = \frac{I_s(t) - \alpha I_p(t)}{I_s(t) + \alpha I_p(t)} \quad (1)$$

where $I_s(t)$ and $I_p(t)$ are fluorescence intensities recorded at time t in the two polarization channels and α is the factor used to balance the two channels, determined by recording isotropic bulk emission. The intensity $I(t)$ is defined as the number of photons per bin of duration 1 ms for Figure 3a,b and duration 100 μs for Figure 3c,d. Figure 4 shows a histogram of the observed A values. The fluorescence bursts were included in Figure 4 only if the sum of the s and p count rates exceeded a threshold, which was carefully selected to ensure that all the background signals were subtracted from the intensity−time record. The histogram in Figure 4 indicates that the mean value

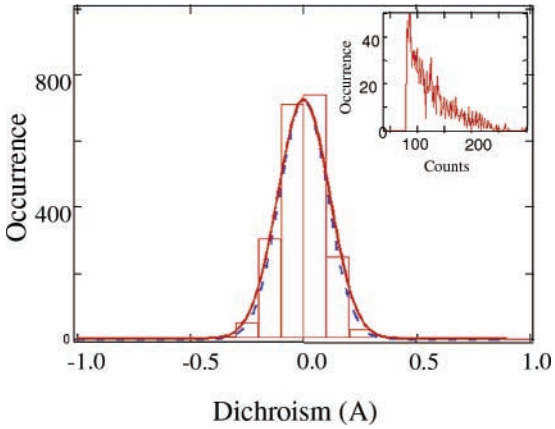

Figure 4. Distribution of dichroism A and the total count distribution (inset) calculated from the data in Figure 3a. Only data for which $I_s(t) + I_p(t) > 80$ were used in the calculation. The solid curve is the best Gaussian fit. The dashed curve shows the calculated distribution of A when shot noise is the only source of deviation from zero of A.

of A is zero. When fitted to a Gaussian, the histogram has a standard deviation of 0.23. The inset of Figure 4 shows the background-subtracted histogram of the total number of counts per bin, $I_s(t) + I_p(t)$, obtained from the complete data set shown in Figure 3a. When normalized, this histogram describes the probability $f(s)$ that a total number of counts s will be obtained in a bin. We can use these data to estimate the distribution of A values that would arise if the molecules were rotating infinitely quickly. For each $f(s)$, the probability $P_s(A)$ that a particular value of A would be measured can be calculated if Poisson statistics and a mean value $\langle A \rangle = 0$ are assumed. The normalized sum of these distributions is the estimate of the dichroism distribution if shot noise is the only source of deviation from $A = 0$. The results, shown via the dashed curve in Figure 4, exhibits a standard deviation of 0.21, which is similar to the experimental result. The same procedures were also used to evaluate the distribution of A of the intensity−time records collected with time bins of 100 μs, and again the observed A has a mean value of zero and standard deviation close to that expected from shot noise. It is concluded that the rotational correlation time is short compared with the binning time of 100 μs.

To further evaluate the effect of patterned surfaces on the rotational diffusion of molecules close to it, we measured the time-resolved fluorescence anisotropy of TMR molecules sandwiched between the patterned surface and a regular cover glass. The confocal microscope was used in these anisotropy experiments, and the laser was focused on the surface of the patterned area to make sure the detected fluorescence signals were only from the molecules close to the patterned surface (the $1/e^2$ radius in the z direction is ~1000 nm, which is the detection depth above the surface). The bulk measurements yield a rotational correlation time of ~1.5 ns, which is consistent with the observations from our single-molecule experiments. The same setup has also been used to measure the rotational correlation time of rhodamine dyes in free solution, where a picosecond time scale rotational correlation time has been found, consistent with previous reports.[40] These measurements indicate the rotational diffusion of molecules close to the patterned surfaces has been slowed compared with that in solution.

The fluorescence intensity fluctuations among bursts and also those within one single burst shown in Figure 3 are influenced by a number of dynamical processes. The laser transverse intensity profile is Gaussian; therefore, the instantaneous excitation and fluorescence intensities will vary depending on the

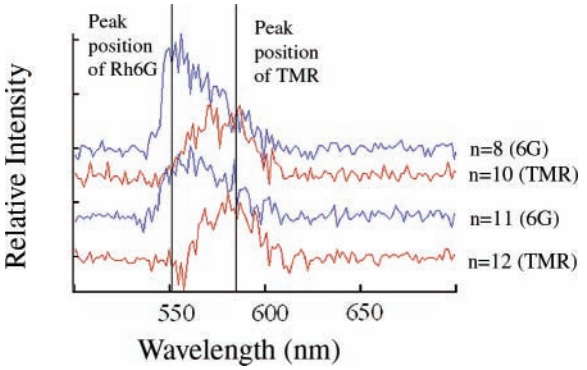

Figure 5. Representative time-resolved fluorescence spectra of fluorescence bursts recorded for the sample with equal concentrations of Rh6G and TMR. The spectra were recorded sequentially, each with an integration time of 500 ms. The label *n* indicates the number in the sequence of the spectra recorded. The $n = 9$ spectrum is not shown here because it only contains a background signal. The two vertical lines indicate the peak positions of Rh6G and TMR. The peak positions, determined under the same experimental conditions but with higher concentrations, are 552 and 575 nm for Rh6G and TMR. All spectra have baselines around zero. The unzeroed baselines for spectra 8, 10, and 11 were created deliberately to show the peak positions clearly.

locations of molecules in the probe volume. For our microscope, the $1/e^2$ radius r and confocal length l are ~260 and ~1000 nm, respectively. The Brownian motion of single molecules in the excitation probe volume is expected to be a major contributor to the fluorescence intensity fluctuations shown in Figure 3. Intersystem crossing from singlet to triplet states can also cause intensity fluctuations[41,42] but is not expected to be a primary contributor in this work. For Rh6G, the intersystem crossing efficiency is ~0.2%, so on average, for every 500 fluorescence cycles, the molecule crosses once into the triplet state. At 1 mW, the fluorescence cycle is ~10 ns and the triplet state lifetime is ~4 μs; therefore, triplet-related dark states occur every 5 μs and have an average duration of ~4 μs. The data would need to be collected with an integration time of ~1 μs in order that the fluorescence intensity fluctuations caused by triplet states be directly observed. For integration times of 100 μs or longer, triplet states are not expected to contribute significantly to the observed fluctuations.

Parts b and d of Figure 3 show expanded versions of the emission bursts indicated by the arrows in Figure 3a,c. Most of the apparent bursts shown in Figure 3a,c actually consist of several shorter bursts separated by brief dark states having durations from 1 to 20 ms, which are comparable with the widths of the bursts. As shown in Figure 3a,c, usually it takes many seconds for another cluster of bursts to appear after the previous one disappears. The intervals between bursts in Figure 3b,d is usually in the range of milliseconds or tens of milliseconds. Therefore, at the 10^{-10} M concentrations used in the present work, clustering of bursts is statistically more likely to be caused by the same molecule recrossing the boundary of the probe volume several times before finally diffusing away. This conclusion is also reached from the analysis of spectral data from mixed samples, which are shown in Figure 5.

To check whether the bursts are from the same molecule continually reentering the probe volume, we carried out experiments with a solution containing equal amounts of the two fluorescent dyes Rh6G and TMR, which have distinguishable fluorescence spectra. The fluorescence spectra of the bursts were recorded on a CCD/monochromator system. The experiment is best described with reference to Figure 3, which is a typical signal. A sequence of ca. 120 spectra were obtained from each time record of this type: the exposure time for a spectrum was

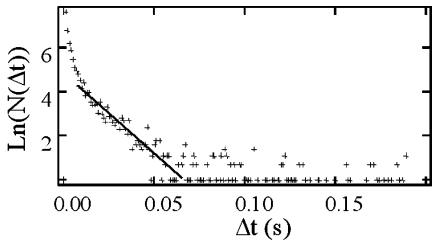

Figure 6. Logarithm of the photon burst interval distribution $N(\Delta t)$ vs time interval Δt. The straight line in the region 10−70 ms represents the best fit to Poisson statistics.

500 ms. From Figure 3 it is evident that for any given 500 ms interval there is a relatively small probability of detecting a burst. In practice about 15% of the 120 sequential attempts showed well-defined spectra above the background. The exposure time of 500 ms easily brackets a 60 ms cluster such as the one shown in Figure 3d. In total we examined 60 sets of 120 spectra. Only ~2% of the individual spectra showed the fluorescence of both dyes. This is consistent with the 1.5% probability calculated from Poisson statistics of two molecules being in the probe volume when the mean number of molecules in the volume is obtained from the concentration of 10^{-10} M. Since the solution contains an equal number of Rh6G and TMR molecules, this result strongly suggests that the clusters of bursts, such as in Figure 3d, correspond to one and the same molecule repeatedly leaving and reentering the probe volume. Roughly the same number of Rh6G and TMR emitting clusters were observed across the complete data set. Figure 5 shows a selection of the spectra obtained in one of the sequences of 120 exposures. In each exposure either Rh6G or TMR is detected. As an additional check we examined the sequences of the spectra of a sample containing only Rh6G. No significant spectral shifts were observed between the different exposures. This confirms that the spectral shifts seen from the mixture are caused by the presence of the different types of dye molecules in the focal volume and not by fluctuations in the spectra of one type of dye.

In Poisson statistics, longer intervals between photon bursts are less probable than shorter intervals and the probability distribution of intervals is expected to be exponential. Figure 6 shows the logarithm of the distribution of intervals $N(\Delta t)$ plotted against the inteval Δt. Figure 6 shows that at longer time intervals ($10 < \Delta t < 60$ ms) the data are described moderately well by Poisson statistics. But for $\Delta t < 10$ ms there is a deviation away from a single-exponential decay. The reentry probability is 6.2 times higher than that predicted by Poisson statistics within the interval of 1−5 ms. The increased reentry probability at short time intervals is typical of optical trapping, which has been reported by Zare and Klenerman.[39,43] However, as discussed below, the laser power in our experiments is much lower than that required for such trapping. Another possibility is that the way the liquid wets the surface in the neighborhood of the cavities forces the molecules that attempt to diffuse away back into the most stable regions.

To explore the diffusion close to the patterned area, we used total internal TIRFM to directly observe movements of single TMR molecules. The penetration depth of the evanescent field is about 150−200 nm, so only molecules close to the surface could be excited. Figure 7 shows the results of some experiments. Figure 7a is the regular sample image obtained by laser illumination without addition of the fluorescent probe. TIRFM images were taken on the same area after addition of 10^{-9} M TMR solution. TMR molecules excited by the evanescent field appear as bright spots on the CCD image. Figure 7b represents

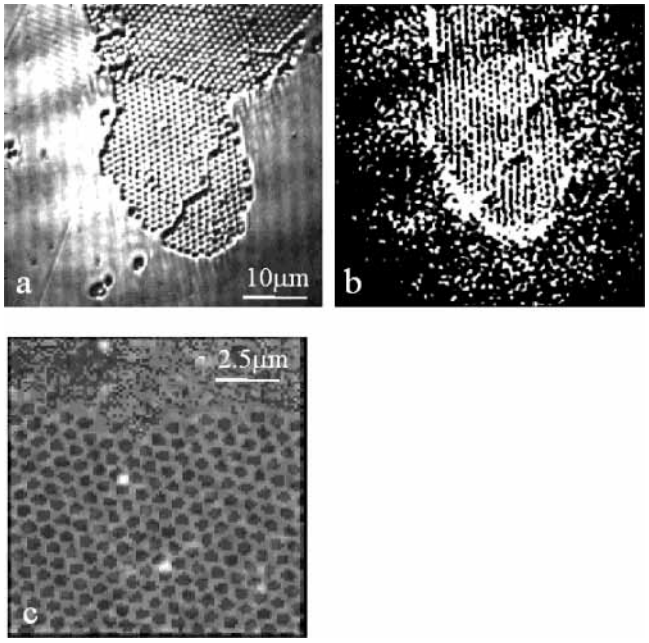

Figure 7. Images obtained by TIRFM. Image a shows the structure of the patterned surface obtained on the CCD camera with laser light illumination. Image b was synthesized by overlapping 500 single-molecule images. For the average all the single-molecule images were obtained from the same patterned area shown in (a). A single-molecule image overlapped with the regular image in (c) shows the diffusion of single molecules near the patterned surface.

an image consisting of 500 frames taken sequentially and superimposed on one another. Surprisingly, molecules are not distributed over the sample uniformly, but follow the structure of the patterned surface. This image suggests that molecules do not diffuse inside the holes. To clarify this phenomenon, we performed another experiment where only a thin layer of TMR solution (hundreds of nanometers) on the sample surface was formed in saturated methanol vapor. In such a preparation, molecules are not free to diffuse away from the sample surface, but are limited to diffuse in the sample plane. We recorded a series of TIRFM images and overlapped them with the regular image of the pattern. Figure 7c is one such image; indeed all molecules in all images such as Figure 7c were observed to be diffusing in the regions between the holes: no molecules were seen to be trapped in the spheroidal cavities.

Autocorrelation Analysis. In fluorescence correlation spectroscopy, which has been widely used to study the diffusion of molecules in solutions,[18,21] the autocorrelation function of the fluorescence intensity of molecules diffusing through the focus of the laser is defined as[18]

$$G(\tau) = \lim\left[\frac{1}{T}\int_0^T S(t)\, S(t+\tau)\right] \qquad (2)$$

where $S(t)$ is the fluorescence intensity detected at time t. The autocorrelation decays from $G(0) = \langle s^2 \rangle$ to $G(\infty) = \langle S \rangle^2$. Figure 8 shows a typical autocorrelation function calculated by using the fluorescence intensity−time records of Figure 3a. The autocorrelation functions were also calculated with data collected at 100 μs binning, and they gave the same result. The accuracy of the diffusion coefficient calculated from single-molecule fluorescence correlation spectroscopy is dependent on the sampling time being less than the residence time, but greater than the time scale of fast dynamics such as intersystem crossing.[44] In the present case, the residence time exceeds 1 ms, so intensity−time records could be collected with 1 ms

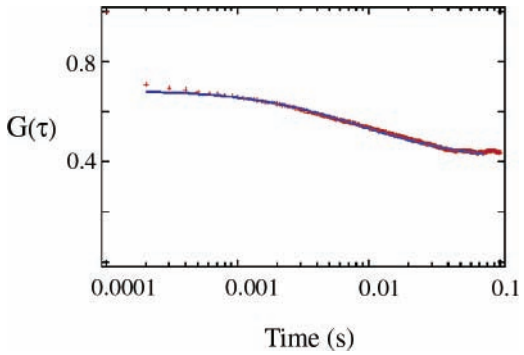

Figure 8. Representative autocorrelation function $G(\tau)$ calculated from the fluorescence intensity−time records of Rh6G. The solid curve is the best fit to a three-dimensional model.

sampling. The measured autocorrelation decay, shown in Figure 8, was fitted by two standard models, one involving diffusion in two and the other in three dimensions.[18,45] We first assumed that detected molecules were diffusing exclusively on the patterned surface, and hence, the decay was fitted to the correlation function for molecules diffusing in and out of the laser beam in a plane representing the patterned surface. The beam was assumed to have a Gaussian transverse profile so that the photon count rate from a molecule depended on its coordinates on the plane. This procedure yielded a best fit diffusion coefficient of 1.7×10^{-8} cm^2 s^{-1}. This would be the appropriate treatment if the only molecules contributing to the signal were those very close to the surface. Another limit is that the emitting molecules are inside the three-dimensional Gaussian intensity profile created by the laser focus (the half-axes of the Gaussian intensity profile in the $x-y$ plane and in the z direction in this case are, respectively, 260 and 1000 nm). This model would be appropriate for the signal that originates from molecules in the liquid between the cover glass and the pattern. This region has a total depth of several micrometers. A diffusion coefficient of 1.8×10^{-8} cm^2 s^{-1} was found by fitting to the correlation function for this case. The molecules diffusing within the laser intensity profile but not close to the surface have much less contribution to the signal because fewer fluorescence photons can be detected from those more rapidly diffusing molecules. The much lower count rate detected for molecules freely diffusing in the solution defined by the three-dimensional Gaussian intensity profile was proven by control experiments with the sample sandwiched directly between two cover glasses, as discussed below and shown in Figure 10. However, the fits to these two- and three-dimensional models are not excellent at short times as can be seen from Figure 8. Better fits over the whole time range could be obtained by assuming both a fast and a slow diffusion, with the former small contribution presumably arising from the molecules in the bulk region. However, the estimate of the surface diffusion, which is the main point of this work, remains unchanged by this type of fitting. The diffusion coefficient of 1.7×10^{-8} cm^2 s^{-1} is approximately 260 times smaller than the translational diffusion coefficient of Rh6G in methanol ($D = 4.5 \times 10^{-6}$ cm^2 s^{-1}).[46] The $G(\tau)$ functions for TMR and TMR−dextran (molecular weight 10K) on the patterned areas created by using 1 μm sized spheres were measured by the same procedures to yield diffusion coefficients of 1.1×10^{-8} and 1.7×10^{-8} cm^2 s^{-1}, respectively, for the three-dimensional correlation function fitting. Similar results were obtained for Rh6G, which has approximately the same hydrodynamic radius as TMR. The similarity of the derived diffusion coefficients for these molecules in the region of patterns made from spheres of different sizes is consistent

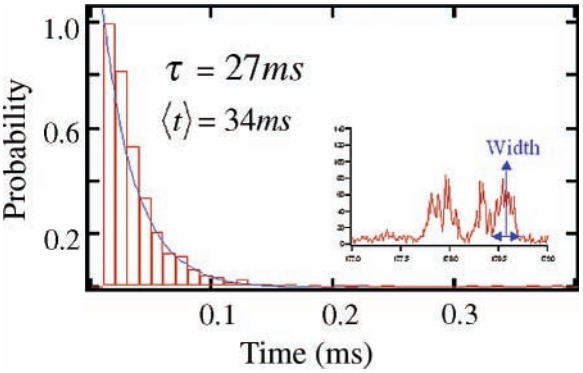

Figure 9. Distribution of the width of the fluorescence bursts. The inset shows the measure of the width. The mean width is 34 ms. The exponential fit yields $\tau = 27$ ms.

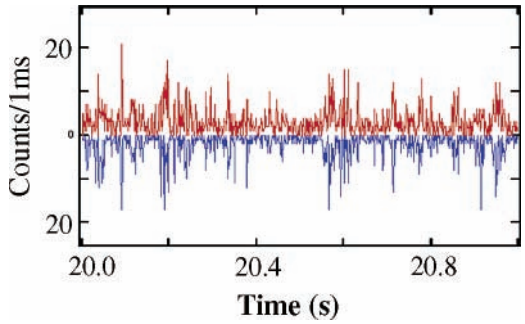

Figure 10. Typical fluorescence intensity−time record of single Rh6G molecules diffusing in a methanol solution sandwiched between two cover glasses (excitation power 50 μW, binning time 1 ms).

with the molecules avoiding the spherical holes. The hydrodynamic radius for 10K dextran is ∼3 nm,[47] which is ∼5 times larger than that of Rh6G ($R = 0.56$ nm for Rh6G).[48] Therefore, the characteristic diffusion time for TMR−dextran was expected to be 5 times longer than for Rh6G or TMR in solution. The similarity of the $G(\tau)$ functions for TMR and TMR−dextran in the present experiment indicates that the dynamics of the lateral motions are not simply predictable from conventional formulas for translational diffusion in solutions. Rather there is some surface control of the tumbling motions on the surfaces.

The residence time of single molecules in the probe volume has also been obtained from direct measurements of the widths of the bursts. Figure 9 shows the distribution of the residence times of single Rh6G molecules near a pattern, created with 0.5 μm spheres. A fit of the distribution to a single exponential yields a mean residence time of 27 ms. The average of all the data in Figure 9 is 34 ms. Both estimates agree well with the results from the autocorrelation analysis.

Samples were also prepared by directly sandwiching 5 μL TMR or Rh6G solutions either between two regular cover glasses or between a PVA-coated cover glass and a regular one. Similar results were obtained from these two samples, typified by the time−intensity record shown in Figure 10 for an incident power of 50 μW. The signal-to-noise ratio and the count rate for the data in Figure 10 are significantly lower than obtained for the data in Figure 3a,b. The difference arises because the residence time of molecules in the probe volume is significantly less than that found for the patterned surfaces. Autocorrelation analysis leads to a diffusion coefficient of 1.6×10^{-6} cm^2 s^{-1}, which is close to that for Rh6G in water. By means of AFM studies, we found that the glass surface is very flat, having only ∼10 nm variations in height across an area of 50 μm^2. The surface of a spin-coated PVA film is rougher than a glass surface but flatter than the patterned surface; it shows 100 nm undulations across an area of 50 μm^2. The diffusion coefficients obtained in these samples indicate that neither glass nor unpatterned polymer surfaces significantly influence the lateral diffusion. Furthermore, in these control experiments the solvent usually evaporated in 5−10 min, whereas the sample in contact with the patterned surface can last much longer. The wall surrounding the pattern (shown in Figure 2) may prevent the solution from evaporating and help to keep solvent in the patterned region.

Generally, the translational diffusion coefficient is proportional to the inverse of the viscosity. The properties of waterlike fluids in micrometer-sized pores have been widely investigated recently.[49−55] Thompson et al.[51] have studied the water confined in cylindrical micropores, which are structurally similar to our templated voids. In their study, they found that, with saturated liquid water outside the pores, the fluid inside the pores is a vapor until the pore radius is increased to a critical size, after which it is a liquid. The critical pore radius is rather large, ∼1500 nm, for hard wall pores, for which the Lennard-Jones potential parameter ϵ_{fw} for the fluid−wall interaction is zero, and becomes much smaller rather dramatically as ϵ_{fw} is increased to ∼2 kJ/mol. For a water−silicate system, $\epsilon_{fw} = 1.422$ kJ/mol,[51] which means, in the presence of bulk liquid outside the pores at ambient conditions, the stable phase inside the silicate pores with radii less than ∼100 nm is predicted to be vapor. ϵ_{fw} for the MeOH−PVA system is not known, but according to this theory the effective viscosity of the fluid in the small spherical holes is unlikely to be larger than that of the bulk solution, whereas we seek a ∼200-fold increase of viscosity to explain the unusually small diffusion coefficient.

Optical trapping can affect the diffusion residence time from its free value of about 0.15 to ∼2 ms when a 0.9 mW laser[39] is focused to the diffraction limit. The maximum excitation power we used was ∼40 μW, so optical trapping should not be responsible for the ∼300 times increase in the residence time observed in our experiments. The data obtained by TIRFM show that molecules are diffusing close to the patterned surface, avoiding the holes. This suggests two possibilities. Perhaps the surface tension, or wetting of the pattern, may result in a slowing of the diffusion. However, we have not established any details of how the lengthening of the residence time is related to the liquid patterns created by those micrometer-sized holes. Another, perhaps related, possibility is that the rough surfaces made at the interfaces of the dissolved spheres are made particularly reactive due to some aspect of the dissolution processes or that they retain solvent after the drying process. Then the molecules may be attached or adsorbed to these edges and tumble along them without ever managing to diffuse into the bulk. Our data indicate that any tumbling process associated with a surface or edge would require the molecule to average its dipole orientation on the nanosecond time scale. As noted earlier the presence of the polymer surface on glass does not cause the extreme slowing of the diffusion that we have found on the patterns. Some future work will be required to address these issues.

In conclusion, nanostructured surfaces have been found to slow the translational diffusion of single molecules while retaining their freedom to rotate faster than the binning time of 100 μs. The rotational averaging occurs on the nanosecond time scale according to bulk measurements on the patterns. The translational diffusion coefficients of TMR, Rh6G, and dextran−TMR diffusing near the patterns are ∼300 times smaller than those in free solution. The slowed diffusion increases the residence time for single molecules in the laser probe volume, which enables an increased amount of spectroscopic information

to be obtained from single fluorescence bursts or clusters of fluorescence bursts from a single molecule. Direct evidence that the cluster of fluorescence bursts is formed by one molecule repeatedly reentering the probe volume has been obtained. Observations by TIRFM have shown that molecules are diffusing around the spheroidal cavities rather than inside them. The detailed mechanism of the diffusion process of single molecules near the patterned surfaces is not clear yet but may be related to the wetting patterns created by the regular array of micrometer-sized cavities and/or to molecules tumbling on the network of rough edges defining the pattern. The goal of immobilizing freely rotating single molecules within the diffraction-limited spot for substantial periods of time is nevertheless accomplished by this technique. However, applications to folded and unfolded proteins and other aqueous systems will require development of an active water-insoluble pattern, which is one avenue of our current research.

Acknowledgment. This work was supported by NIH Research Resource Grant P41 RR001348 and NIH Grant PO1 48130. R.M.H. is indebted to the European Laser Laboratory (LENS) for their hospitality while this paper was being completed.

References and Notes

(1) Moerner, W. E.; Kador, L. *Phys. Rev. Lett.* **1989**, *62*, 2535.
(2) Basche, T.; Moerner, W. E. *Nature* **1992**, *355*, 335.
(3) Ambrose, W. P.; Moerner, W. E. *Nature* **1991**, *349*, 225.
(4) Betzig, E.; Chichester, R. J. *Science* **1993**, *262*, 1422.
(5) Nie, S.; Chiu, D. T.; Zare, R. N. *Science* **1994**, *266*, 1018.
(6) Dunn, R. C.; Holtom, G. R.; Mets, L.; Xie, X. S. *J. Phys. Chem.* **1994**, *98*, 3094.
(7) Funatsu, T.; Harada, Y.; Tokunaga, M.; Saito, K.; Yanagida, T. *Nature* **1995**, *374*, 555.
(8) Ha, T.; Enderle, T.; Ogletree, D. F.; Chemla, D. S.; Selvin, P. R.; Weiss, S. *Proc. Natl. Acad. Sci. U.S.A.* **1996**, *93*, 6264.
(9) Mei, E.; Tang, J.; Vanderkooi, J. M.; Hochstrasser, R. M. *J. Am. Chem. Soc.* **2003**, *125*, 2730.
(10) Bopp, M. A.; Jia, Y. W.; Li, L. Q.; Cogdell, R. J.; Hochstrasser, R. M. *Proc. Natl. Acad. Sci. U.S.A.* **1997**, *94*, 10630.
(11) Schuler, B.; Lipman, E. A.; Eaton, W. A. *Nature* **2002**, *419*, 743.
(12) Lipman, E. A.; Schuler, B.; Bakajin, O.; Eaton, W. A. *Science* **2003**, *301*, 1233.
(13) Lee, M.; Tang, J.; Hochstrasser, R. M. *Chem. Phys. Lett.* **2001**, *344*, 501.
(14) Hou, Y.; Bardo, A. M.; Martinez, C.; Higgins, D. A. *J. Phys. Chem. B* **2000**, *104*, 212.
(15) Rhoades, E.; Gussakovsky, E.; Haran, G. *Proc. Natl. Acad. Sci. U.S.A.* **2003**, *100*, 3197.
(16) Lu, H. P.; Xie, X. S. *Nature* **1997**, *385*, 143.
(17) Talaga, D. S.; Lau, W. L.; Roder, H.; Tang, J.; Jia, Y.; DeGrado, W. F.; Hochstrasser, R. M. *Proc. Natl. Acad. Sci. U.S.A.* **2000**, *97*, 13021.
(18) Eigen, M.; Rigler, R. *Proc. Natl. Acad. Sci. U.S.A.* **1994**, *91*, 5740.
(19) Ehrenberg, M.; Rigler, R. *J. Chem. Phys.* **1974**, *4*, 390.
(20) Magde, D.; Elson, E. L.; Webb, W. W. *Biopolymers* **1974**, *13*, 29.
(21) Wirth, M. J.; Swinton, D. J.; Ludes, M. D. *J. Phys. Chem. B* **2003**, *107*, 6258.
(22) Daniel, D. C.; Thompson, M.; Woodbury, N. W. *J. Phys. Chem. B* **2000**, *104*, 1382.
(23) Deniz, A. A.; Laurence, T. A.; Beligere, G. S.; Dahan, M.; Martin, A. B.; Chemla, D. S.; Dawson, P. E.; Schultz, P. G.; Weiss, S. *Proc. Natl. Acad. Sci. U.S.A.* **2000**, *97*, 5179.
(24) Grunwell, J. R.; Glass, J. L.; Lacoste, T. D.; Deniz, A. A.; Chemla, D. S.; Schultz, P. G. *J. Am. Chem. Soc.* **2001**, *123*, 4295.
(25) Nie, S.; Chiu, D. T.; Zare, R. N. *Anal. Chem.* **1995**, *67*, 2849.
(26) Kollner, M.; Wolfrum, J. *Chem. Phys. Lett.* **1992**, *27*, 199.
(27) Yu, J.; Hu, D.; Barbara, P. F. *Science* **2000**, *289*, 13271330.
(28) Deschenes, L. A.; Vanden Bout, D. A. *Science* **2001**, *292*, 255.
(29) Hofkens, J.; Maus, M.; Gensch, T.; Vosch, T.; Cotlet, M.; Kohn, F.; Herrmann, A.; Mullen, K.; Schryver, F. D. *J. Am. Chem. Soc.* **2000**, *122*, 9278.
(30) Mei, E.; Bardo, A. M.; Collinson, M. M.; Higgins, D. A. *J. Phys. Chem. B* **2000**, *104*, 9973.
(31) Luther, B. J.; Springer, G. H.; Higgins, D. A. *Chem. Mater.* **2001**, *13*, 2281.
(32) Holland, B. T.; Blanford, C. F.; Stein, A. *Science* **1998**, *281*, 538.
(33) Johnson, S. A.; Ollivier, P. J.; Mallouk, T. E. *Science* **1999**, *283*, 963.
(34) Jiang, P.; Hwang, K. S.; Mittleman, D. M.; Bertone, J. F.; Colvin, V. L. *J. Am. Chem. Soc.* **1999**, *121*, 11630.
(35) Park, S. H.; Xia, Y. *Chem. Mater.* **1998**, *10*, 1745.
(36) Nykypanchuk, D.; Strey, H. H.; Hoagland, D. A. *Science* **2002**, *297*, 987.
(37) Bopp, M. A.; Sytnik, A.; Howard, T. D.; Cogdell, R. J.; Hochstrasser, R. M. *Proc. Natl. Acad. Sci. U.S.A.* **1999**, *96*, 11271.
(38) Kiefer, J.; Hilborn, J. G.; Hedrick, J. L. *Polymer* **1996**, *37*, 5715.
(39) Osborne, M. A.; Balasubramanian, S.; Furey, W. S.; Klenerman, D. *J. Phys. Chem. B* **1998**, *102*, 3160.
(40) Schaffer, J.; Volkmer, A.; Eggeling, C.; Subramaniam, V.; Striker, G.; Seidel, C. A. M. *J. Phys. Chem. A* **1999**, *103*, 331.
(41) Yip, W.-T.; Hu, D.; Yu, J.; Vanden Bout, D. A.; Barbara, P. F. *J. Phys. Chem.* **1998**, *102*, 7564.
(42) Weston, K. D.; Carson, P. J.; Metiu, H.; Buratto, S. K. *J. Chem. Phys.* **1998**, *109*, 7474.
(43) Chiu, D. T.; Zare, R. N. *J. Am. Chem. Soc.* **1996**, *118*, 6512.
(44) Gell, C.; Brockwell, D. J.; Beddard, G. S.; Radford, S. E.; Kalverda, A. P.; Smith, D. A. *Single Mol.* **2001**, *2*, 177.
(45) Elson, E. L.; Magde, D. *Biopolymers* **1974**, *13*, 1.
(46) Hansen, R. L.; Zhu, X. R.; Harris, J. M. *Anal. Chem.* **1998**, *70*, 1281.
(47) Ioan, C. E.; Aberle, T.; Burchard, W. *Macromolecules* **2000**, *33*, 5730.
(48) Karolin, J.; Geddes, C. D.; Wynne, K.; Birch, D. J. S. *Meas. Sci. Technol.* **2002**, *13*, 21.
(49) Raviv, U.; Laurat, P.; Klein, J. *Nature* **2001**, *413*, 51.
(50) Marti, J.; Gordillo, M. C. *Chem. Phys. Lett.* **2002**, *354*, 227.
(51) Giaya, A.; Thompson, R. W. *J. Chem. Phys.* **2002**, *117*, 3464.
(52) Allen, R.; Melchionna, S.; Hansen, J.-P. *Phys. Rev. Lett.* **2002**, *89*, 175502.
(53) Marti, J.; Guardia, E.; Gordillo, M. C. *Chem. Phys. Lett.* **2002**, *365*, 536.
(54) Truskett, T. M.; Debenedetti, P. G.; Torquato, S. *J. Chem. Phys.* **2001**, *114*, 2401.
(55) Soper, A. K.; Bruni, F.; Ricci, M. A. *J. Chem. Phys.* **1998**, *109*, 1486.